AECL-9112

ATOMIC ENERGY OF CANADA LIMITED

L'ÉNERGIE ATOMIQUE DU CANADA LIMITÉE

THE ELECTRON TEST ACCELERATOR BEAM INJECTOR

L'injecteur à faisceau d'un accélérateur d'électron test

J.-P. LABRIE and R.T.F. BIRD

Chalk River Nuclear Laboratories

Laboratoires nucléaires de Chalk River

Chalk River, Ontario

April 1986 avril

ATOMIC ENERGY OF CANADA LIMITED

THE ELECTRON TEST ACCELERATOR BEAM INJECTOR

J.-P. Labrie and R.T.F. Bird

Accelerator Physics Branch
Chalk River Nuclear Laboratories
Chalk River, Ontario, Canada K0J 1J0

1986 April

AECL-9112

L'ENERGIE ATOMIQUE DE CANADA, LIMITEE

L'injecteur à faisceau d'un accélérateur d'électron test

par

J.P. Labrie et R.T.F. Bird

Résumé

Un système de pulsation de faisceau et un système de groupeur pour faisceau ont été conçus afin d'améliorer d'efficacité de capture et de réduire l'écoulement du faisceau dans l'accélérateur d'électron test. Le groupeur pour faisceau augmente la capture DC de faisceau de 30 à 70%. Une transmission de faisceau à 100% à travers les structures de l'accélérateur est obtenue avec le système de pulsation de faisceau. Ce rapport décrit les résultats des tests expérimentaux avec l'injecteur de faisceau. Les résultats de modélisation par ordinateur et des mesures avec des prototypes qui ont conduit à la conception d'un système de pulsation de faisceau et système de groupeur de faisceau sont discutés.

Département de la Physique des Accélérateurs
Laboratoires Nucléaire de Chalk River
Chalk River, Ontario K0J 1J0

1986 Avril

AECL-9112

ATOMIC ENERGY OF CANADA LIMITED

THE ELECTRON TEST ACCELERATOR BEAM INJECTOR

J.-P. Labrie and R.T.F. Bird

Abstract

beam chopper and buncher system has been designed to improve the capture fficiency and reduce the beam spill in the Electron Test Accelerator. The uncher increases the dc beam capture from 30 to 70%. 100% beam transmission hrough the accelerator structures is obtained with the chopper. This report escribes results of experimental tests with the beam injector. Results from omputer modeling and from measurements with prototypes that have led to the esign of the beam chopper and buncher system are discussed.

Accelerator Physics Branch
Chalk River Nuclear Laboratories
Chalk River, Ontario, Canada K0J 1J0

1986 April

AECL-9112

1. INTRODUCTION

The Electron Test Accelerator (ETA) was designed as an electron model of the coupled cavity section of a high power proton accelerator for electronuclear breeding[1]. Figure 1 shows a sketch of ETA. The continuous wave (cw) linear accelerator is composed of two side-coupled structures operating at 805 MHz. Each structure is driven with a 100 kW VA-850 klystron. Electrons from a triode gun operated at 85 kV traverse a matching section before being injected into a graded-β* structure having its cavity lengths graded so that as the velocity of the electrons increases, synchronism with the accelerating fields is maintained. Electrons emerging from this capture section have an energy of 1.5 MeV and at these relativistic energies, they can be further accelerated to 4 MeV in the second, constant cavity length, structure with almost 100% transmission.

The dc beam transmission through the graded-β structure was improved from 30% to 70% by bunching the beam in the injector line and beam currents up to 20 mA have been accelerated in the 0° beam line. Beam spill in the graded-β structure and in the first dipole magnet limited the beam current to less than 1 mA at the electron window in the 45° beam line and in the 90° beam line where new accelerator concepts are being developed[2].

To reduce beam spill in the accelerator a high current injector beam line has been designed to chop and bunch the dc beam from the electron gun. This new injector beam line, shown in Fig. 2, is designed to dissipate up to 20 kW of electron beam power at an energy of 85 keV. In addition to the triode electron gun, the injector beam line is composed of three gap lenses, a beam deflecting cavity, a buncher cavity, a drift space, high power slits, a wire scanner, coils for background magnetic field suppression and beam steering. This report describes the performance of the beam chopper and buncher system and gives results of measurements with prototype devices that have lead to the construction of the high current ETA injector.

---

* β is the usual relativistic velocity parameter.
β = particle velocity divided by the velocity of light.

2. DESIGN OF THE BEAM CHOPPER AND BUNCHER SYSTEM

2.1 Operating Principles

The purpose of a beam chopper is to transform the dc beam from the electron gun into longitudinal bunches with a repetition rate at a harmonic of the frequency of rf fields in the accelerator structures. This is accomplished by sweeping the dc beam across slits with a chopper cavity. The width of the slits and the power in the chopper cavity define the phase spread of the bunches injected in the accelerator structures.

Further beam density modulation is obtained from velocity modulation of the dc beam in a buncher cavity operating at a harmonic of the frequency of accelerating fields in the structures, followed by a beam drift. The drift distance, width of slits and phase of the fields in the chopper and buncher with respect to the fields in the graded-β structure are arranged to match the high beam density regions to the admittance of the accelerator.

The calculated admittance[3] in the energy-phase plane of the graded-β structure is shown in Fig. 3. As the β of the electrons injected into the capture section approaches unity, the acceptance phase range increases. At an injection energy of 85 keV, the acceptance phase range is 190°. The chopper and buncher system is designed to minimize the beam spill in the accelerator by injecting a narrow phase spread bunched beam into the acceptance phase range of the graded-β structure (see Fig. 3).

Two constraints were imposed on the design of the beam chopper system: the available space in the ETA tunnel and the operating frequency of the accelerator (805 MHz). The space constraint limits the drift lengths and has imposed the injector beam line configuration shown in Fig. 4. A beam chopper system with a single deflecting cavity usually operates at one half the accelerator frequency. The beam is then swept across the slits once per accelerator rf cycle. In our case, the beam deflecting cavity frequency is the same as the accelerator to minimize component cost. This constraint implies, as shown in

Fig. 5, that for each rf cycle, the beam is swept twice across the slits. Part of the beam is decelerated and lost in the first accelerating cavity. In Fig. 5, the dc beam length AE represents 360° (19.17 mm at 85 keV) and intermediate points, B, C and D are separated by 90°. The chopper folds AE over the aperture while the buncher compresses B and D towards C. The slits select the phase spread of the beam injected in the graded-β linac.

2.2 Beam Chopper System

2.2.1 Prototype Chopper Cavity

A cylindrical cavity operating in the TM_{110} mode was chosen to deflect the beam. The TM_{110} mode has two orthogonal components in a cylindrical cavity which are almost degenerate. Mode separator plates were installed in a cylindrical cavity to shift the frequency of the orthogonal components sufficiently apart to eliminate coupling between the x and y axes (z being defined as the beam axis).

An aluminum prototype of a chopper cavity operating in the TM_{110} mode at a frequency of 2450 MHz was constructed. The cavity profile, shown in Fig. 6, was optimized with the computer code URMEL[4] for electrons with an energy of 85 keV. The prototype cavity has a plunger for frequency control, is driven with a magnetic field coupling loop and has an electric field pick-up probe.

The reasons for constructing the prototype cavity were:

(1) To measure the tuning range of the TM_{110} mode with a plunger located in the magnetic field region.

(2) To measure the field distribution of the TM_{110} mode and ensure that displacements of the tuner did not introduce changes in the mode spacial configuration.

(3) To examine higher order modes, in particular those close to the second harmonic of the TM_{110} mode.

The wave length of the TM_{110} mode in a cylindrical resonator of radius a is given by

$$\lambda = 1.64\ a. \tag{1}$$

The frequency shift resulting from a change in the cavity temperature, ΔT, is then

$$\frac{\Delta f}{f} = - \Delta T \frac{1}{a} \frac{\Delta a}{\Delta T}. \tag{2}$$

The range of a tuner required to correct for frequency shifts from temperature changes is about ± 0.1% of the drive frequency. Results of measurements of the frequency of the TM_{110} mode as a function of the tuner position, shown in Fig. 7, indicate that the tuner could shift the TM_{110} mode frequency by ± 0.3%.

Over the measured frequency range, the Q value of the TM_{110} mode is constant within 6% (this is within the accuracy of the measurements) and the coupling of the drive loop is independent of the tuner position. This behaviour is different from that observed for the TM_{010} mode in cylindrical resonators and may result from the field distributions within each "kidney" of the TM_{110} mode being, to some extent, independent of one another, as will be seen later.

Magnetic field distribution was measured at the outer perimeter of the cavity by inserting radially at different azimuthal points a 1 mm diameter metal wire and observing the resulting frequency increase. Electric field distribution was measured in the beam aperture region with a 1 mm diameter dielectric rod inserted through the cavity at different azimuthal positions parallel to the symmetry axis and observing the resulting decrease in frequency. This allowed the electric and the magnetic fields both present in this region of the cavity to be measured separately.

Measurements were made at 2451 MHz and 2456 MHz, corresponding to the tuner fully retracted to the outer perimeter of the cavity, and fully inserted, respectively. The square root of the measured frequency shift is proportional to the magnetic and electric fields and results are shown in Figs. 8 and 9. The azimuthal dependence of both magnetic and electric field varies as sin ϕ and the full curves on Figs. 8 and 9 are the predicted field distribution for the TM_{110} mode in a cylindrical cavity. Because the metal wire is inserted radially in the cavity at its outer perimeter, the contribution of the electric field, which is perpendicular to the wire, is negligible and the measured frequency shift are related to the magnetic field.

The magnetic field distributions shown in Fig. 8 indicate that the tuner affects only locally the field distribution in one of the "kidneys" of the TM_{110} mode. The perturbation is not significantly propagated in the beam aperture region as seen from the electric field distributions shown in Fig. 9. The tuner does not introduce measurable changes in the field orientation.

The TM_{110} mode is azimuthally degenerate in an ideal cylindrical cavity. In the aluminum test cavity, this degeneracy is lifted by the position of the magnetic field coupling loop, the electric field pick-up probe and the mode separators. The mode separators are used to decouple the x and y components of the TM_{110} mode. These shift the orthogonal mode frequency by more than 100 MHz.

The frequency of higher order modes and of modes excited in the orthogonal position was measured for different penetrations of the tuning plunger in the cavity. Higher order mode frequencies were not found close to the lower harmonics of the drive frequency indicating that the chopper cavity is excited almost exclusively in the desired TM_{110} beam deflecting mode.

2.2.2 Beam Deflection System

The deflection angle of on-axis particles traversing a cylindrical cavity excited in the TM_{110} mode is given by the ratio of transverse momentum imparted by the magnetic field in the cavity to the longitudinal momentum of the particles. This ratio can be related to easily measured cavity parameters. The maximum deflection angle of on-axis particles is given by

$$\alpha = \tan^{-1} 1.11 \times 10^{-5} \frac{1}{\gamma} \sqrt{PQ \frac{\lambda}{h}} \sin\left(\frac{\pi h}{\beta\lambda}\right) \qquad (3)$$

where P is the power in watts dissipated in a cylindrical cavity of length h excited in the TM_{110} mode having a wave length λ and quality factor Q. γ is the ratio of the particle total energy to its rest mass energy.

Figure 10 shows a photograph of the 805 MHz OFHC copper beam deflecting cavity. The inner cavity dimensions are scaled from the aluminum prototype shown in Fig. 6. The outer cavity diameter is 479 mm and the overall length along the beam axis is 210 mm. Stainless steel end plates 10 mm thick, containing the water cooling channels, were brazed on 5 mm thick OFHC copper to keep the end plate deflection under atmospheric load to less than 0.35 mm^5, producing a frequency shift of -3 kHz when bringing the cavity under vacuum.

The Q of the beam deflecting cavity after brazing is 21 150, 27% less than the value predicted with URMEL. The difference is attributed to the power dissipated in the electric field probe and the tuning plunger assembly which can not be calculated with URMEL. For on-axis electrons injected at an energy of 85 keV, the maximum deflection angle imparted by the beam deflecting cavity (eqn. 3) is

$$\alpha = \tan^{-1} 2.74 \times 10^{-3} \sqrt{P} \qquad (4)$$

High power slits are used to intercept part of the beam and select the phase spread of the beam injected into the graded-β linac. The slit opening required for an injected beam phase spread, $\Delta\phi$, is given by

$$\Delta x = 2.74 \times 10^{-3} \frac{\Delta\phi}{90^\circ} L \sqrt{P} \qquad (5)$$

where L is the distance between the beam deflecting cavity and the slits and P the power dissipated in the cavity. For example, a slit opening of 3 mm is required for an injected beam phase spread of 10° if 100 W is dissipated in the beam deflecting cavity located at 1 m from the slits.

2.3 Beam Buncher System

Figure 11 shows the profile of the 805 MHz buncher cavity operating in the TM_{010} mode and optimized with SUPERFISH[6] for 85 keV electrons. The measured Q and effective shunt impedance of the buncher cavity after brazing are 16 100 and 28 MΩ/m. The difference from the Q value and effective shunt impedance of 22 500 and 35 MΩ/m calculated with SUPERFISH is attributed to losses in the tuner assembly and in the field probe.

The phase compression obtained from the velocity modulation of a dc beam with a buncher cavity of length h after a drift distance L is given by[7]

$$\Delta\phi = \frac{2\pi L}{\beta\lambda} \frac{1}{\gamma^2 + \gamma} \frac{\sqrt{ZT^2\, P\, h}}{T} \qquad (6)$$

where ZT^2 is the effective shunt impedance of the cavity, P is the power dissipated in the cavity and T is the kinetic energy of the injected beam.

For our buncher cavity, optimum bunching occurs at a power level of 30 W and after a drift space of 1 m.

The relative beam current distribution can be calculated from the relationship[7]

$$\frac{I_2}{I_0} = \left(1 - \frac{2\pi L}{\gamma}\left(\gamma^2 - 1\right)^{-3/2} \frac{\sqrt{ZT^2\ P\ h}}{m_0 c^2} \cos \phi_1\right)^{-1} \qquad (7)$$

where m_0c^2 and ϕ_1 are the particle rest mass energy and input phase respectively. An example of the calculated relative beam current distribution at optimum bunching is shown on Fig. 12. Hatched regions correspond to the beam transmitted through the chopper and buncher system when the slits associated with the chopper system are set for a beam phase spread of 40° at the input of the graded-β linac. Note that the calculations indicate that the bunched beam accepted into the graded-β linac is reduced from 83% of the dc beam without chopper to 11% with the chopper set for a 40° beam phase spread.

2.4 Longitudinal Beam Dynamics Calculation for ETA

2.4.1 Impulse Approximation

Longitudinal beam dynamics calculations were made to determine the beam energy resolution and phase spread of ETA. The system configuration is shown in Fig. 13. It is composed of a 85 keV dc electron gun, followed by a beam deflecting cavity, a buncher cavity, a drift space, a graded-β linac with its bridge (Model 4), a second drift space and finally a β=1 linac section with its bridge (Model 3).

Since only on-axis particles are considered, the inclusion of the beam deflecting cavity in the system is relevant only in terms of the behaviour of the longitudinal matching to Model 4 and Model 3 for a given energy resolution and phase spread at the output of ETA.

In the impulse approximation, the energy gain (or loss) experienced by a particle traversing a rf cavity is assumed to occur at the center of the cavity. The algorithm used throughout our calculations is as follows:

(i) For each cavity, the phase of a particle, $\phi(1)$, and its beta, $\beta(1)$, at the input of the cavity, are used to calculate the phase at the center of the cavity. If the length of a cavity is CL, the phase of a particle at its center is

$$\phi(2) = \phi(1) + 360 \frac{CL}{2} \frac{1}{\beta(1)\lambda} \tag{8}$$

where λ is the wave length.

(ii) The energy of the particle at the center of the cavity becomes

$$W(2) = W(1) + E_0 T\ CL \sin \phi(2) \tag{9}$$

where W(1) is the particle's energy at the input of the cavity, E_0 is the average field on-axis and T is the transit time factor.

(iii) The energy of the particle (eqn. 9) is used to calculate the particle's new beta, $\beta(2)$, and the phase of the particle at the output of the cavity is obtained from

$$\phi(3) = \phi(2) + 360 \frac{CL}{2} \frac{1}{\beta(2)\lambda} \tag{10}$$

Results from this algorithm have been compared with particle dynamics calculations for on-axis particles using the computer code PARMELA[8]. In PARMELA, a Fourier expansion of the field distribution in a rf cavity is used. Space charge forces have little effect at beam currents below 200 mA and the agreement with PARMELA results for on-axis particles is within 10%. The parameters for ETA relevant to our calculations are given in Table I.

2.4.2 Results

(A) Longitudinal Matching Section

The longitudinal matching section is composed of the beam deflecting cavity, the buncher cavity, a drift space and a set of slits. The longitudinal characteristics of the beam at optimum bunching are shown in Fig. 14. The phase compression, defined as the ratio of the phase extension at the end of the drift space to an initial phase extension is as large as 9.5.

The combined action of the buncher and chopper must be taken into account in describing the beam injected into the graded-β structure. The chopper cavity scans a beam that is further velocity modulated by the buncher. From the bunching characteristics shown in Fig. 14, an output phase spread of 20° centered around the particle unaffected by the buncher corresponds to an input phase spread of 40°. Consequently by setting the variable slits associated with the beam chopper system to a phase spread of 20°, a beam with a phase spread of 40° will be transmitted through the matching section and compressed to 20° before being injected into Model 4.

(B) Graded-β Linac

The output energy phase diagram at the output of Model 4 is shown in Fig. 15. At an injection energy of 85 keV, the phase acceptance of Model 4 is 190° (see Fig. 3), over which the output energy varies by 15%.

(C) β=1 Linac

The output energy phase diagram at the output of Model 3 is shown in Fig. 16. The phase acceptance of Model 3 is similar to that of Model 4 (in the calculation, the output of Model 4 is injected into Model 3) and the energy spread at the output of Model 3 is very sensitive to the phase between Model 4 and Model 3. This corresponds to transforming phase

spread into energy spread and vice-versa. For a phase difference of -140° between the two structures, the energy spread at the output of Model 3 is 7.5% and the transmission of the dc beam through both structures is 31% (a value comparable to that measured).

Reducing the phase spread at the input of Model 4 will reduce the energy spread at the output of Model 3. Some examples are given in Table II. The energy spread at the output of Model 3 can be reduced to 1% if the phase spread at the input of Model 4 is less than 20°. This in turn corresponds to allowing less than 40° (or less than 11%) of the dc beam to be transmitted through the longitudinal matching section and accelerated by Model 4 and Model 3. The transmission through both structures will be close to 100% (some off-axis particles may be lost). Hence a 10 mA beam at the output of Model 3 would require a gun capable of delivering a 100 mA beam.

3. BEAM TESTS OF THE CHOPPER AND BUNCHER SYSTEM

3.1 Beam Deflection

Beam deflections obtained with the chopper cavity were measured at various rf power levels from changes in the dc beam transverse width. A wire scanner located at 1 m from the chopper cavity was used to measure the width of the beam and Fig. 17 shows the observed increase in beam width as a function of the power dissipated in the cavity. The results indicate that the measured maximum beam deflection angle is given by

$$\alpha = \tan^{-1} (2.56 \pm 0.30) \times 10^{-3} \sqrt{P} \qquad (11)$$

where P is the power in watts. This is in good agreement with the maximum deflection calculated from eqn. (4) for on-axis particles.

3.2 Transmission through the Graded-β Structure

The transmission through ETA graded-β linac structure was measured as a function of the phase spread of the injected beam. The opening of the high power slits associated with the chopper system was set for injecting a bunched beam with a fixed phase spread into the graded-β structure. The phase of the fields in the graded-β structure relative to the chopper and buncher system was varied. Figure 18 shows the transmitted beam as a function of the phase between the fields in the graded-β structure and the injector for two input beam phase spread. Results confirm our calculations that the phase admittance of Model 4 for electrons injected at 85 keV exceeds 100°. However, 100% transmission is obtained only if the input beam phase spread is less than 45°.

3.3 Output Beam Energy Spread and Beam Transmission through ETA

The first 45° dipole magnet and the pair of high power slits located in the 45° beam line (see Fig. 1) were used in an attempt to measure the FWHM beam energy spread as a function of the beam phase spread at the injector. Results shown in Fig. 19 are inconclusive because the energy instabilities of the accelerator of about 50 keV[9] dominated our measurements.

Without chopping, transmission of a bunched beam through the accelerator to the irradiation window in the 45° beam line is about 30% and 40% of the input beam is lost in the accelerator. Using the chopper and buncher system set for a 40° input beam phase spread, 100% transmission through the accelerator to the irradiation window is obtained, corresponding to 11% transmission of the dc beam from the gun, in excellent agreement with the results of our longitudinal beam dynamics calculation.

4. CONCLUSION

A high current injector line has been designed for ETA. The injector line comprises a beam chopper and buncher system which allows for 100% transmission of the injected beam through the accelerator, utilizing 11% of the beam from the gun. Results of experimental tests are in excellent agreement with the calculated behaviour of the system.

ACKNOWLEDGMENTS

Contributions to the design and fabrication of components for the beam chopper and buncher system were made by J.E. Anderchek, R.J. Bakewell, H. Euteneuer (University of Mainz, West Germany), S. Gowans and D.G. Hewitt. Their participation is gratefully acknowledged.

REFERENCES

1. S.O. Schriber, "Canadian Accelerator Breeder System Development", Atomic Energy of Canada Limited, Report AECL-7840 (1982).

2. J.-P. Labrie, K.C.D. Chan and J. McKeown, "The Chalk River Electron Accelerator; A Prototype for Industrial Accelerator Designs", IEEE Trans. Nucl. Sci., NS-30 (2), 1634 (1983).

3. J.S. Fraser, S.H. Kidner, J. McKeown and G.E. McMichael, "The Chalk River Electron Test Accelerator", Proc. of the 1972 Proton Linear Accelerator Conference, LA-5115, 226 (1972).

4. T. Weiland, October 1982, unpublished report.

5. Calculations of end wall deflections were made assuming a circular plate with a concentric hole, fixed at the outer edge and under a constant load of 101.3 kPa. W. Griffel, "Handbook of Formulas for Stress and Strain", Frederick Ungar Publishing Co., New York (1966).

6. K.H. Halbach and R.F. Holsinger, "SUPERFISH - A Computer Program for Evaluation of RF Cavities with Cylindrical Symmetry", Particle Accelerators 7, 213 (1976).

7. J. Haimson, "Some Aspects of Electron Beam Optics and X-Ray Production with the Linear Accelerator", IEEE Trans. Nucl. Sci., NS-9 (2), 32 (1962).

8. K.R. Crandall, private communication.

9. D.E. Earle, private communication.

Table I

Electron Test Accelerator Cavity Parameters

Model 4 Graded-β Structure

Cavity Number	Length (m)	Average On-axis Field (MV/m)	Transit Time Factor
1	0.1147	1.200	0.8790
2	0.1370	1.132	0.8447
3	0.1505	1.068	0.8278
4	0.1591	1.062	0.8183
5	0.1649	1.054	0.8126
6	0.1691	1.050	0.8068
Bridge	0.5123		
7	0.1721	1.014	0.8058
8	0.1744	0.960	0.8038
9	0.1762	0.958	0.8022
10	0.1776	1.020	0.8010
11	0.1787	1.073	0.8001

Model 3 β=1 Structure

1 to 9	0.18625	0.9768	0.7940
Bridge	0.565		
10 to 18	0.18625	0.9768	0.7940

Table II

Effects of the Beam Chopper System on the Energy and Phase Spread of the Beam at the Output of ETA

Input Phase Spread* (degree)	Output Energy Spread (%)	Output Phase Spread (degree)
360	7.5	33
80	2.5	26
60	2.5	18
40	2.0	11
20	1.0	6

* Phase spread at the input of Model 4.

Table I

Electron Test Accelerator Cavity Parameters

Model 4 Graded-β Structure

Cavity Number	Length (m)	Average On-axis Field (MV/m)	Transit Time Factor
1	0.1147	1.200	0.8790
2	0.1370	1.132	0.8447
3	0.1505	1.068	0.8278
4	0.1591	1.062	0.8183
5	0.1649	1.054	0.8126
6	0.1691	1.050	0.8068
Bridge	0.5123		
7	0.1721	1.014	0.8058
8	0.1744	0.960	0.8038
9	0.1762	0.958	0.8022
10	0.1776	1.020	0.8010
11	0.1787	1.073	0.8001

Model 3 β=1 Structure

1 to 9	0.18625	0.9768	0.7940
Bridge	0.565		
10 to 18	0.18625	0.9768	0.7940

Table II

Effects of the Beam Chopper System on the Energy and Phase Spread of the Beam at the Output of ETA

Input Phase Spread* (degree)	Output Energy Spread (%)	Output Phase Spread (degree)
360	7.5	33
80	2.5	26
60	2.5	18
40	2.0	11
20	1.0	6

* Phase spread at the input of Model 4.

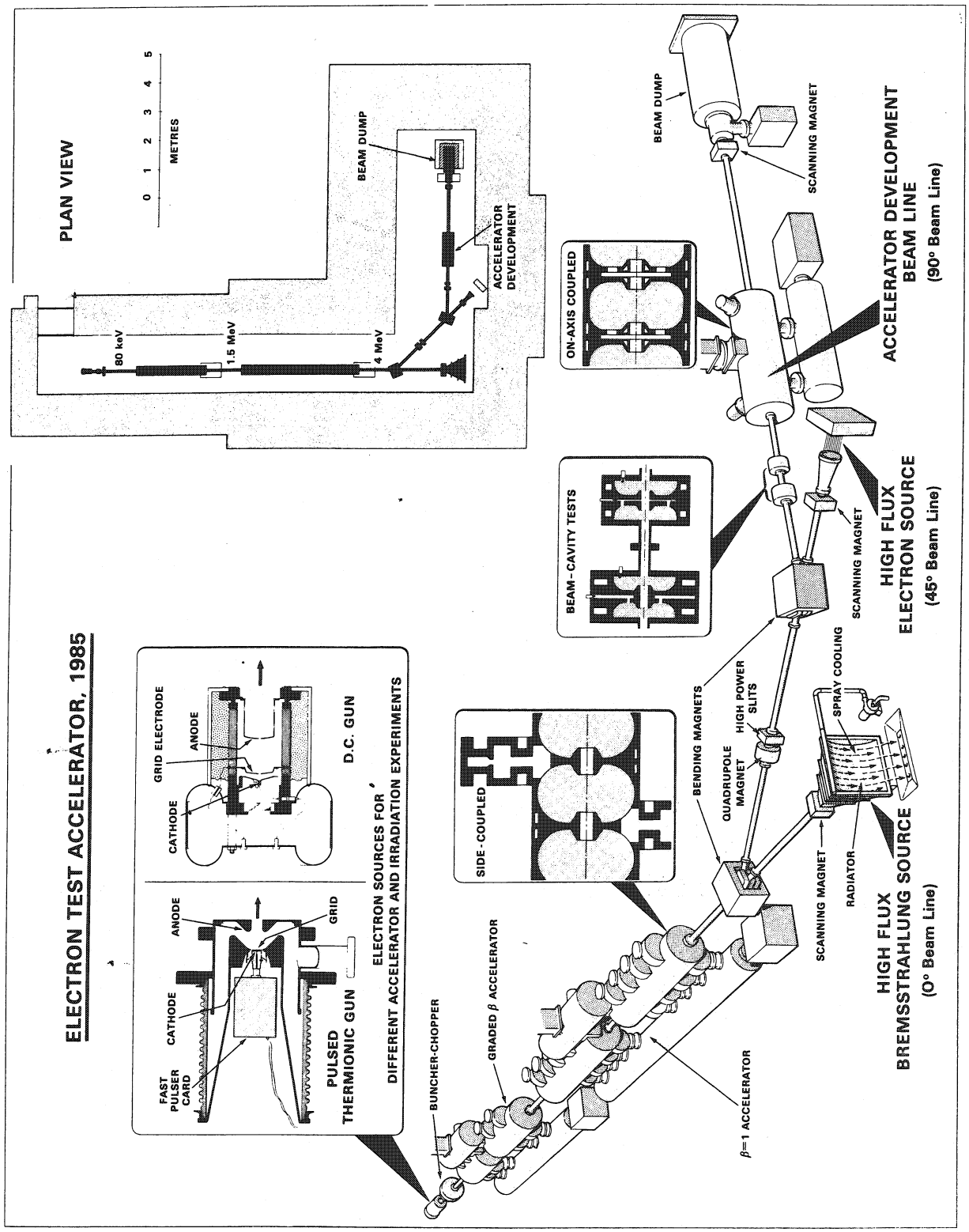

Fig. 1 The Chalk River Electron Test Accelerator.

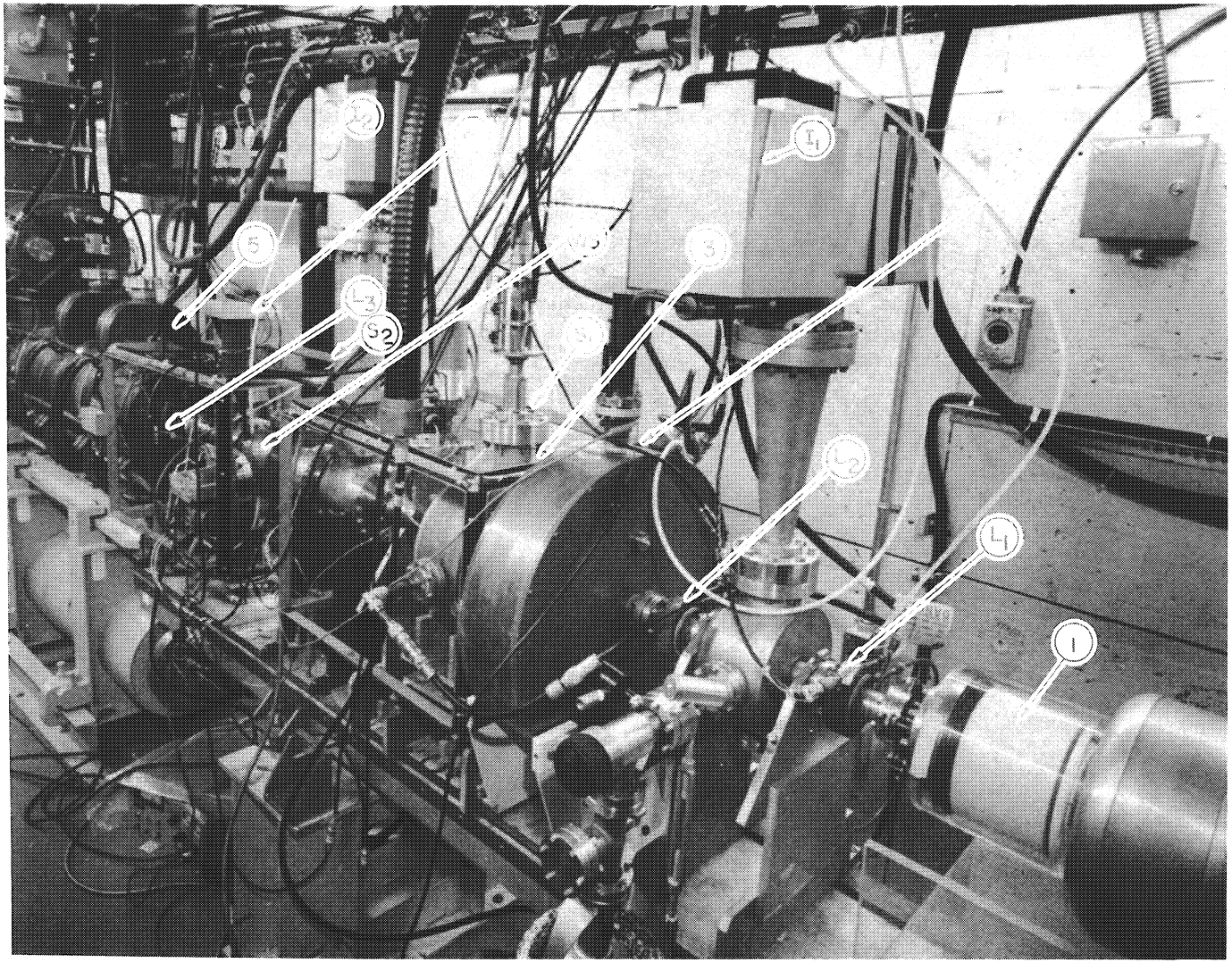

Fig. 2 The Electron Test Accelerator high current injector. (1) Electron gun, (2) beam chopper cavity, (3) beam buncher cavity, (4) high power slits, (5) graded-β accelerator structure, (L_1 to L_3) gap lenses, (S_1 to S_2) background magnetic field suppression and beam steering coils, (I_1 - I_2) ion pumps, (WS) wire scanner.

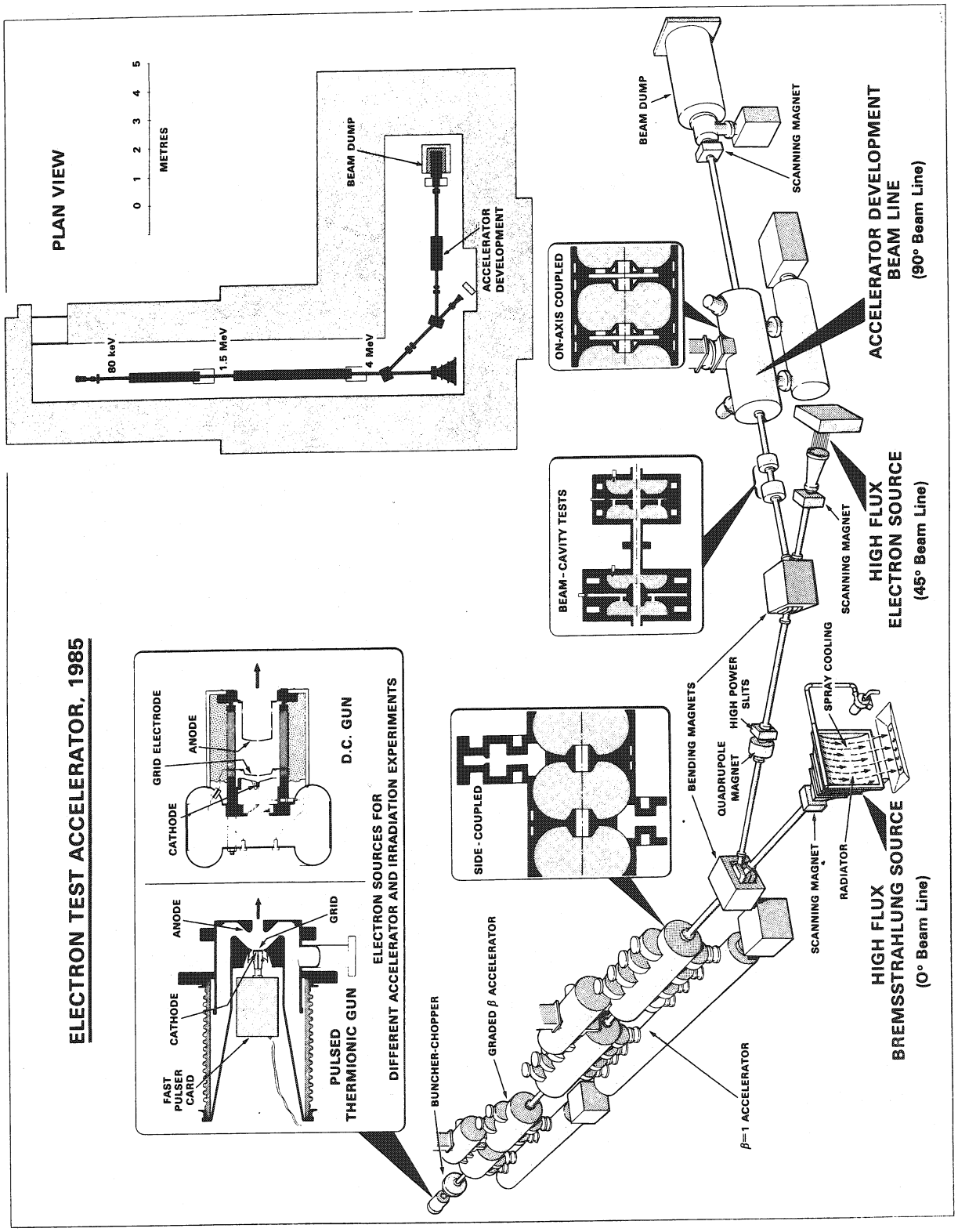

Fig. 1 The Chalk River Electron Test Accelerator.

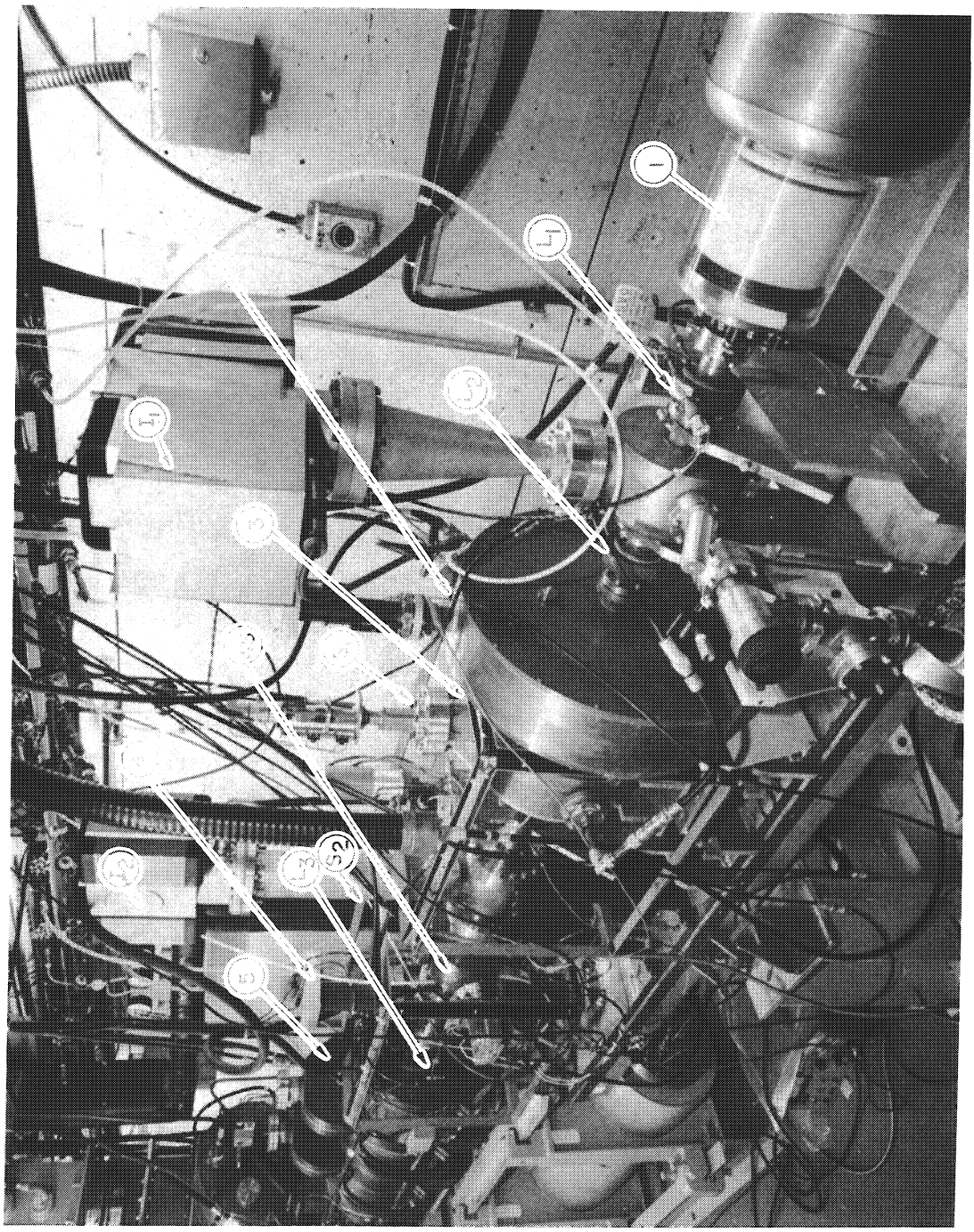

Fig. 2 The Electron Test Accelerator high current injector. (1) Electron gun, (2) beam chopper cavity, (3) beam buncher cavity, (4) high power slits, (5) graded-β accelerator structure, (L_1 to L_3) gap lenses, (S_1 to S_2) background magnetic field suppression and beam steering coils, (I_1 - I_2) ion pumps, (WS) wire scanner.

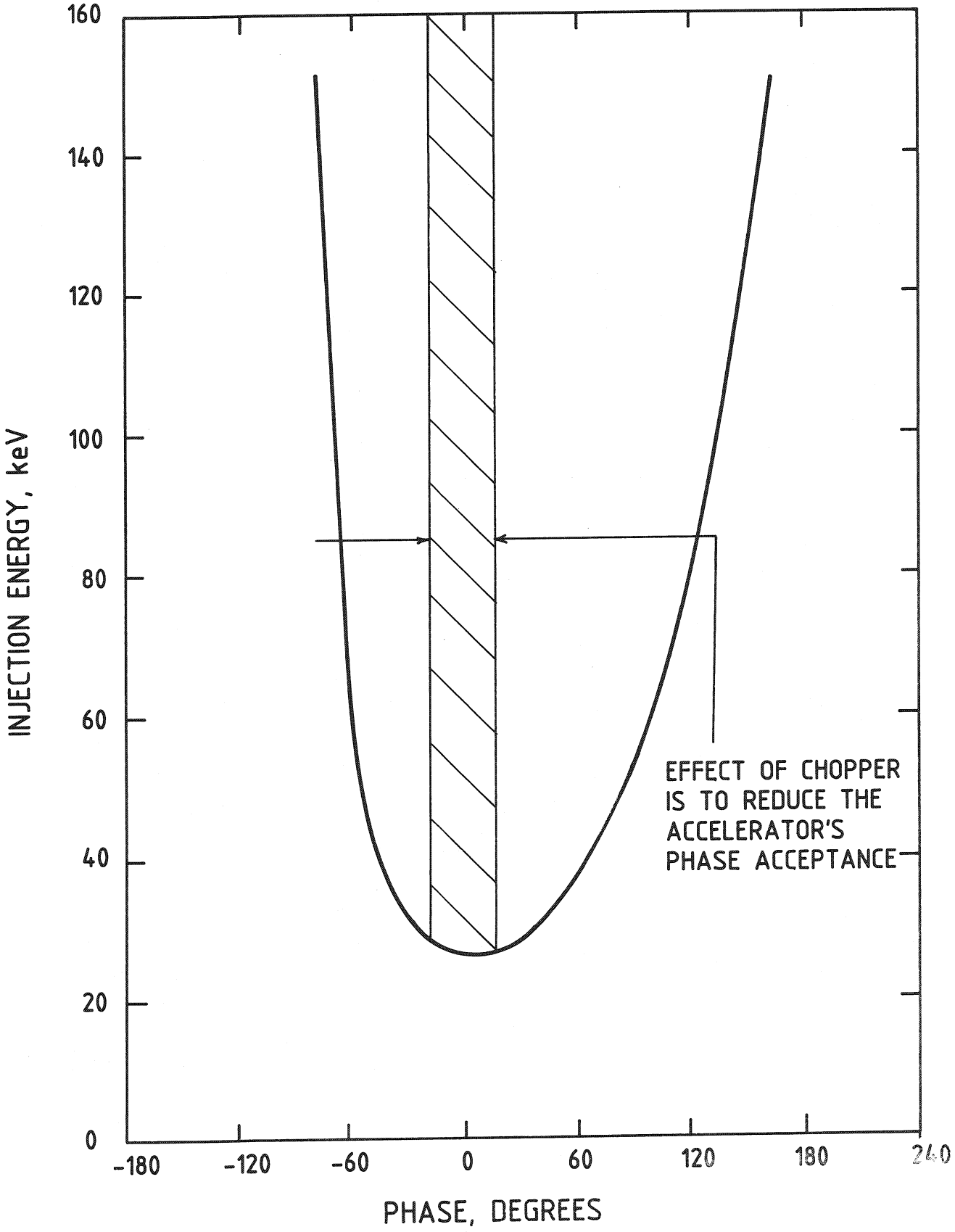

Fig. 3 Calculated longitudinal admittance of the ETA graded-β structure.

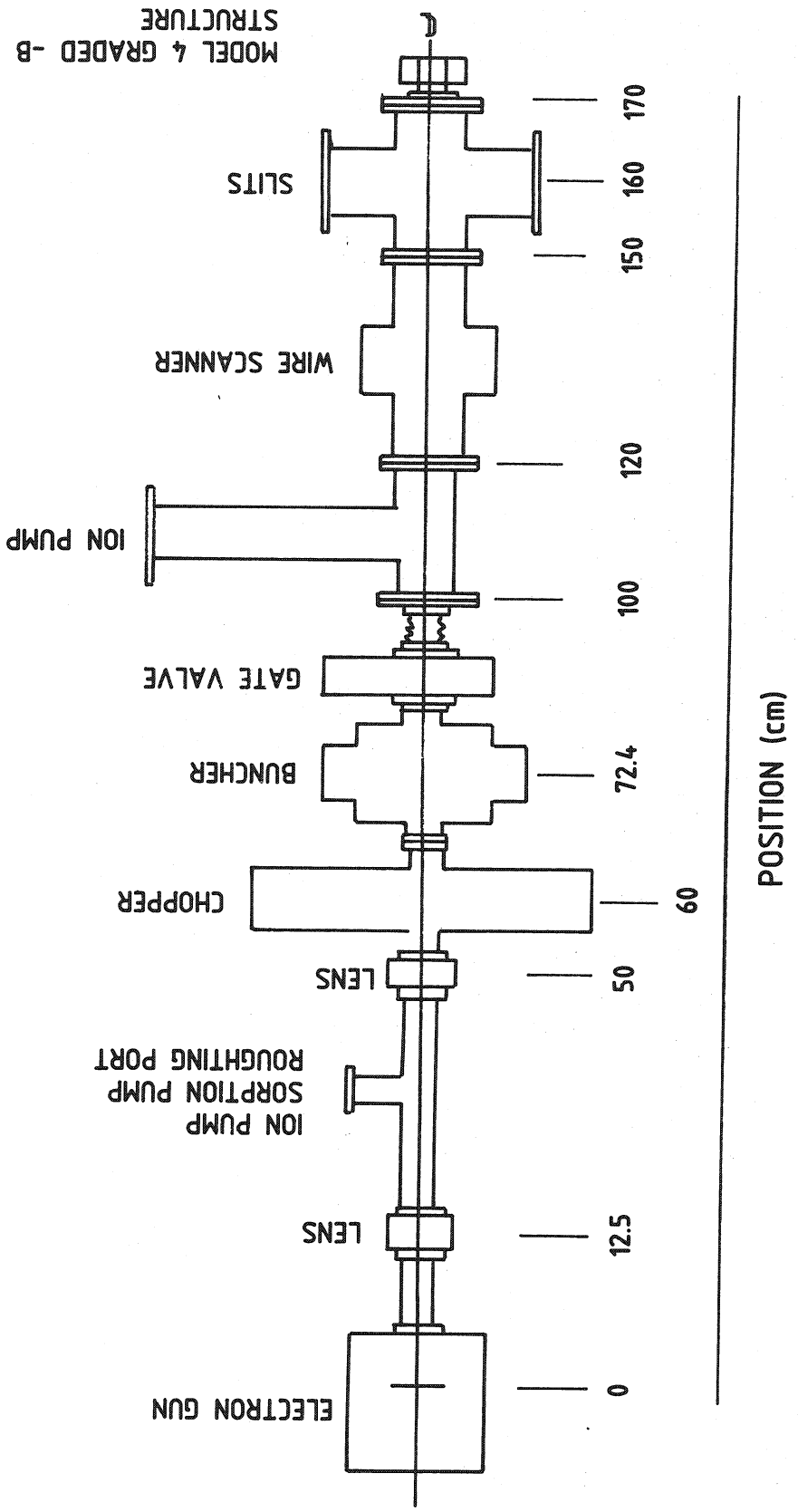

Fig. 4 Injector beam line configuration.

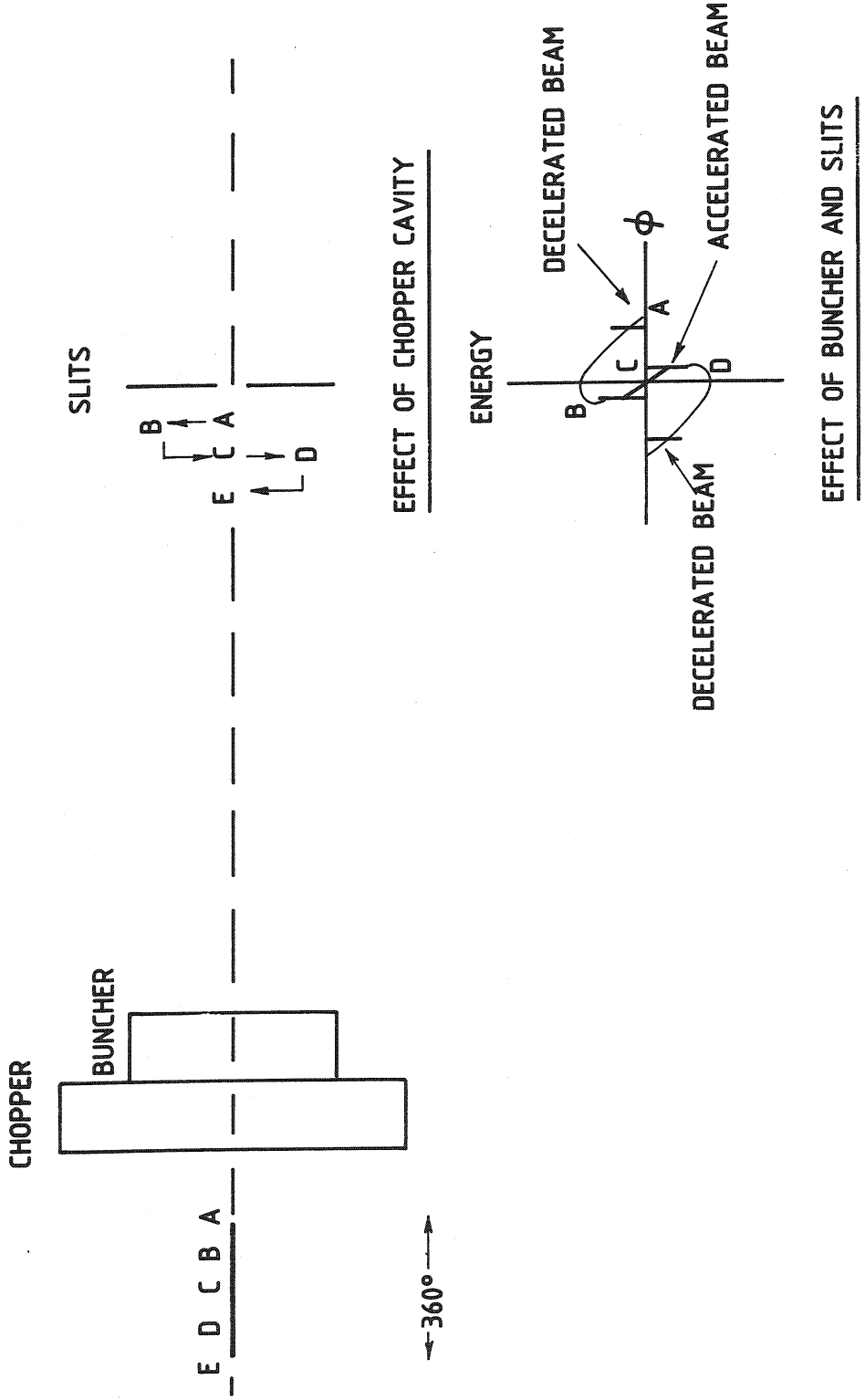

Fig. 5 Operation principle of the longitudinal matching section.

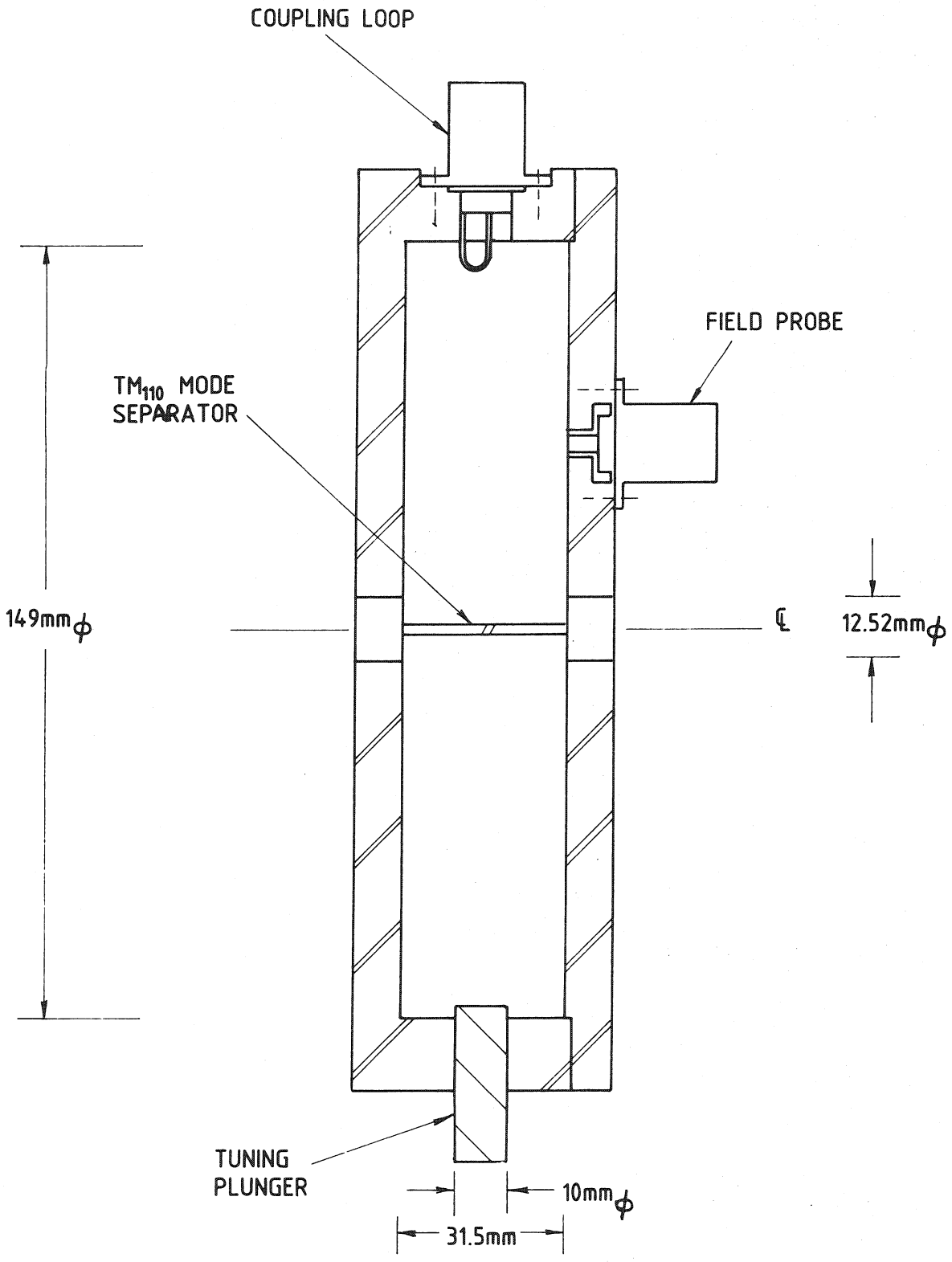

Fig. 6 Beam deflecting cavity prototype operating in the TM_{110} mode at 2450 MHz.

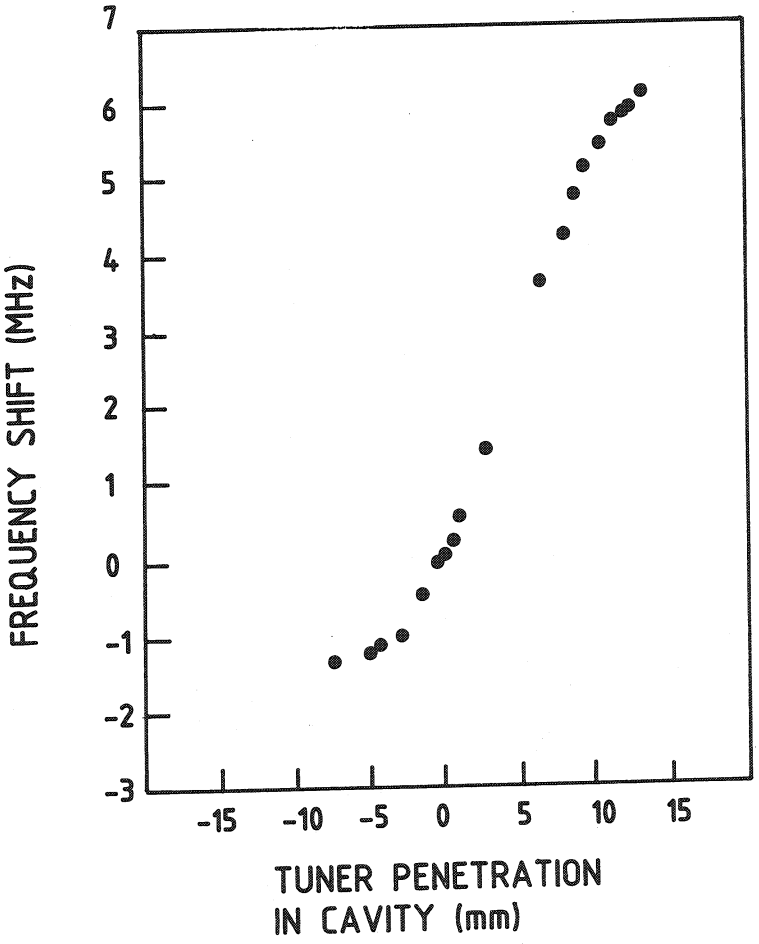

Fig. 7 Frequency range of tuning plunger in prototype beam chopper cavity.

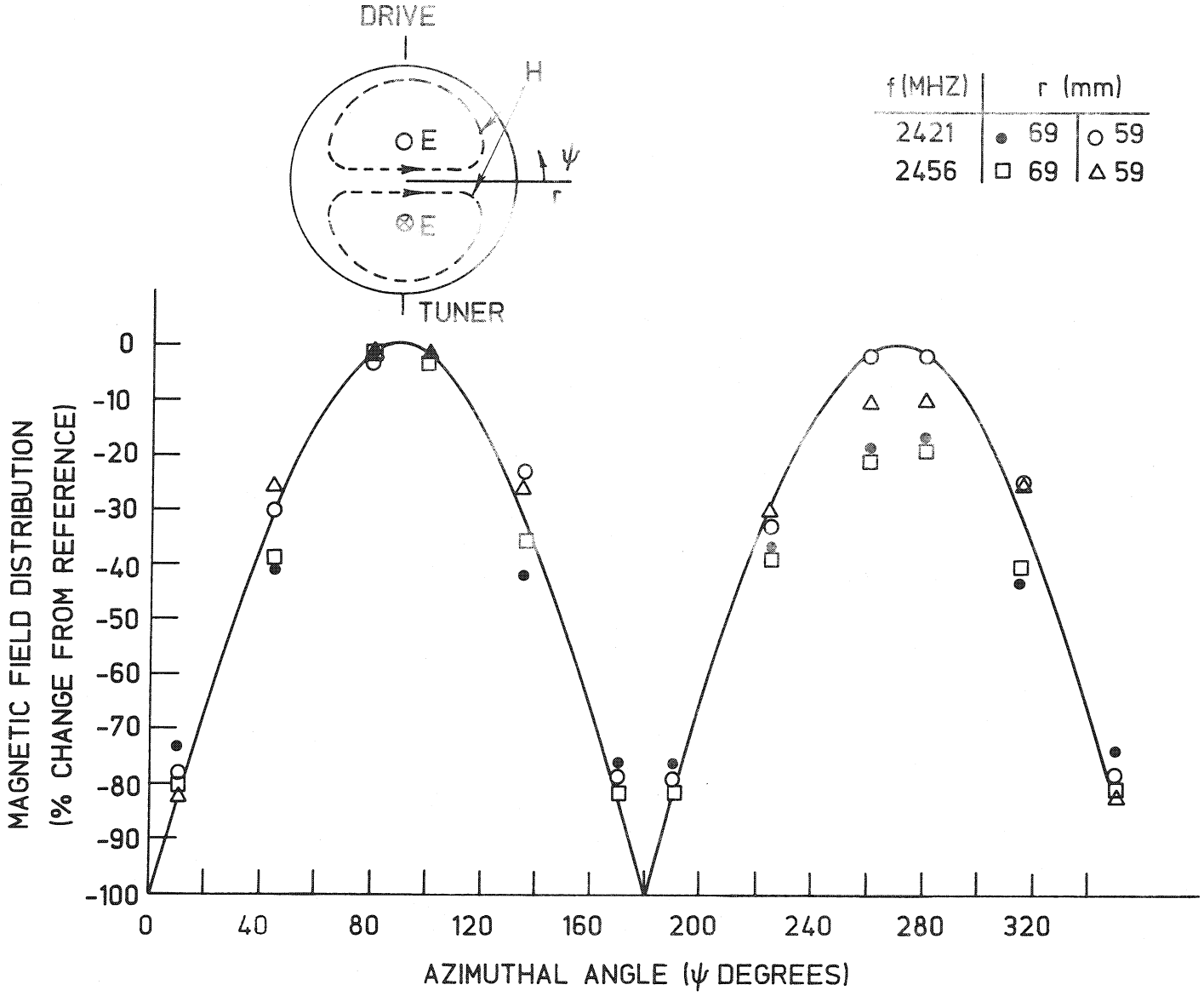

Fig. 8 TM_{110} magnetic field distribution.

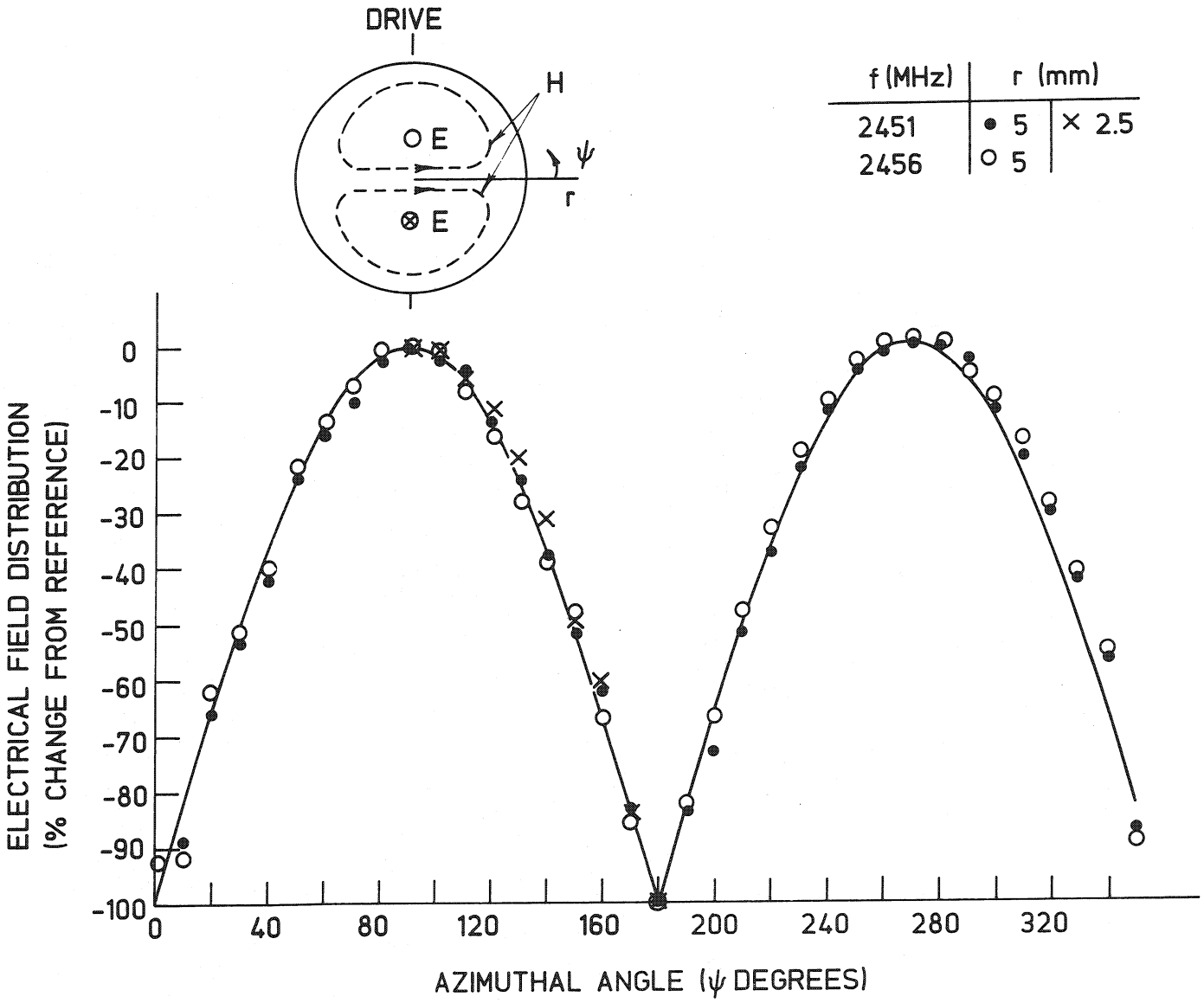

Fig. 9 TM_{110} electric field distribution.

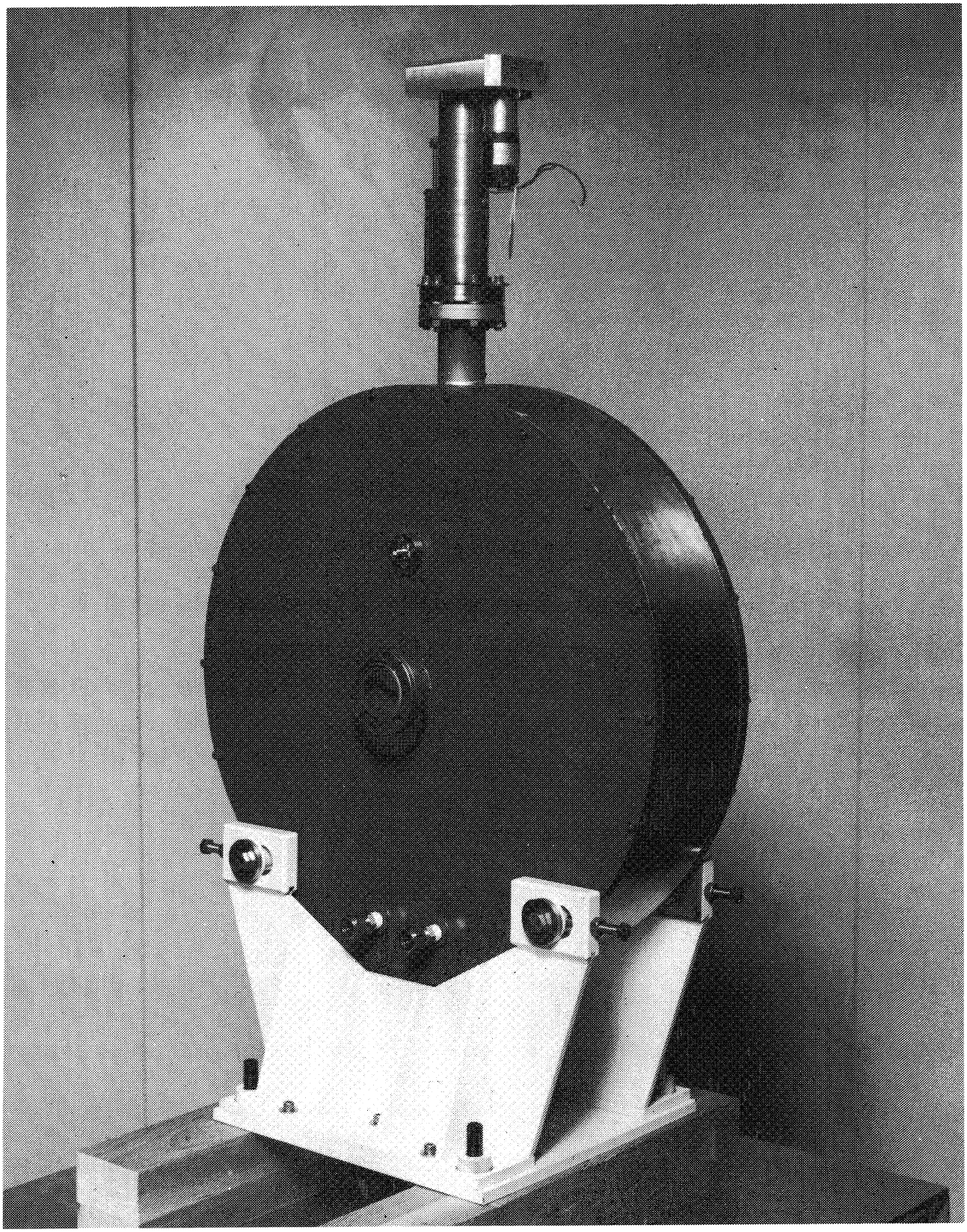

Fig. 10 Beam deflecting cavity operating at 805 MHz in the TM_{110} mode.

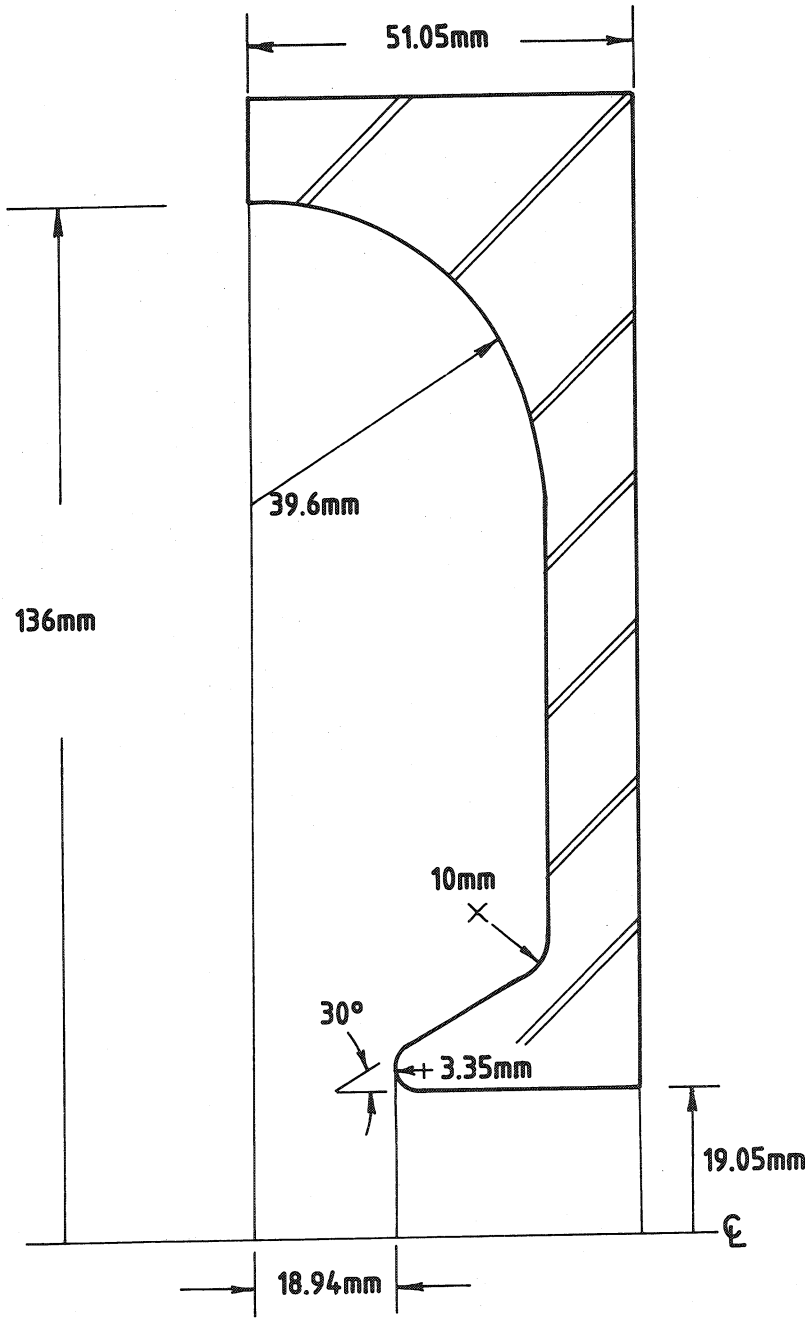

Fig. 11 Profile of the 805 MHz buncher cavity.

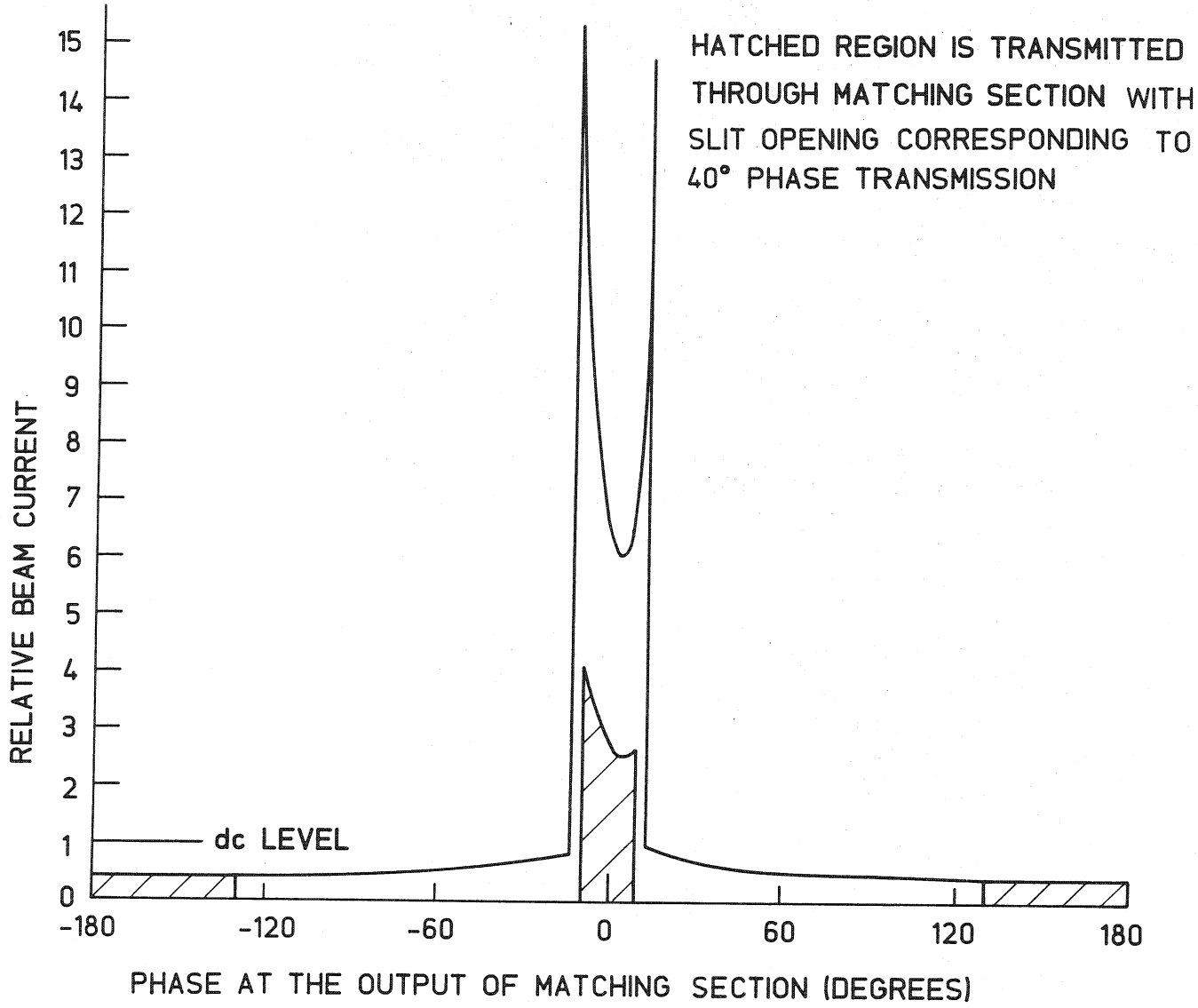

Fig. 12 Calculated beam characteristics at optimum bunching. Hatched regions show the transmission through the injector with the chopper system set for a beam phase spread of 40°.

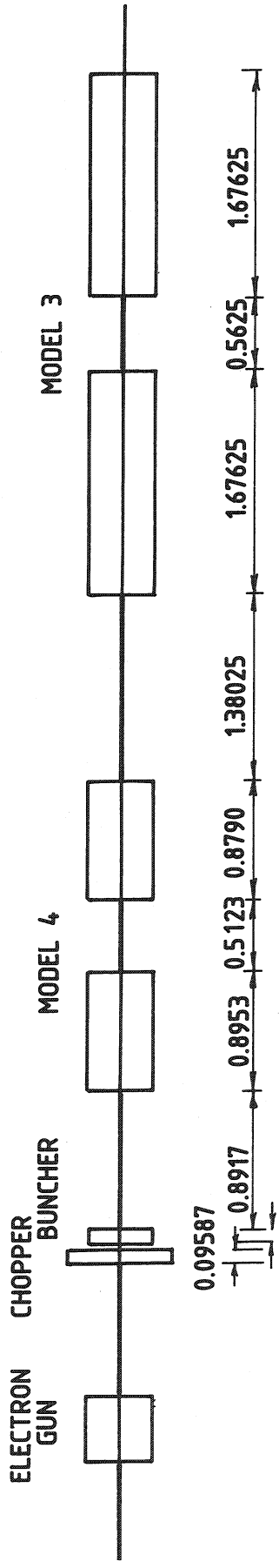

Fig. 13 Configuration of the Electron Test Accelerator. All lengths are given in metre.

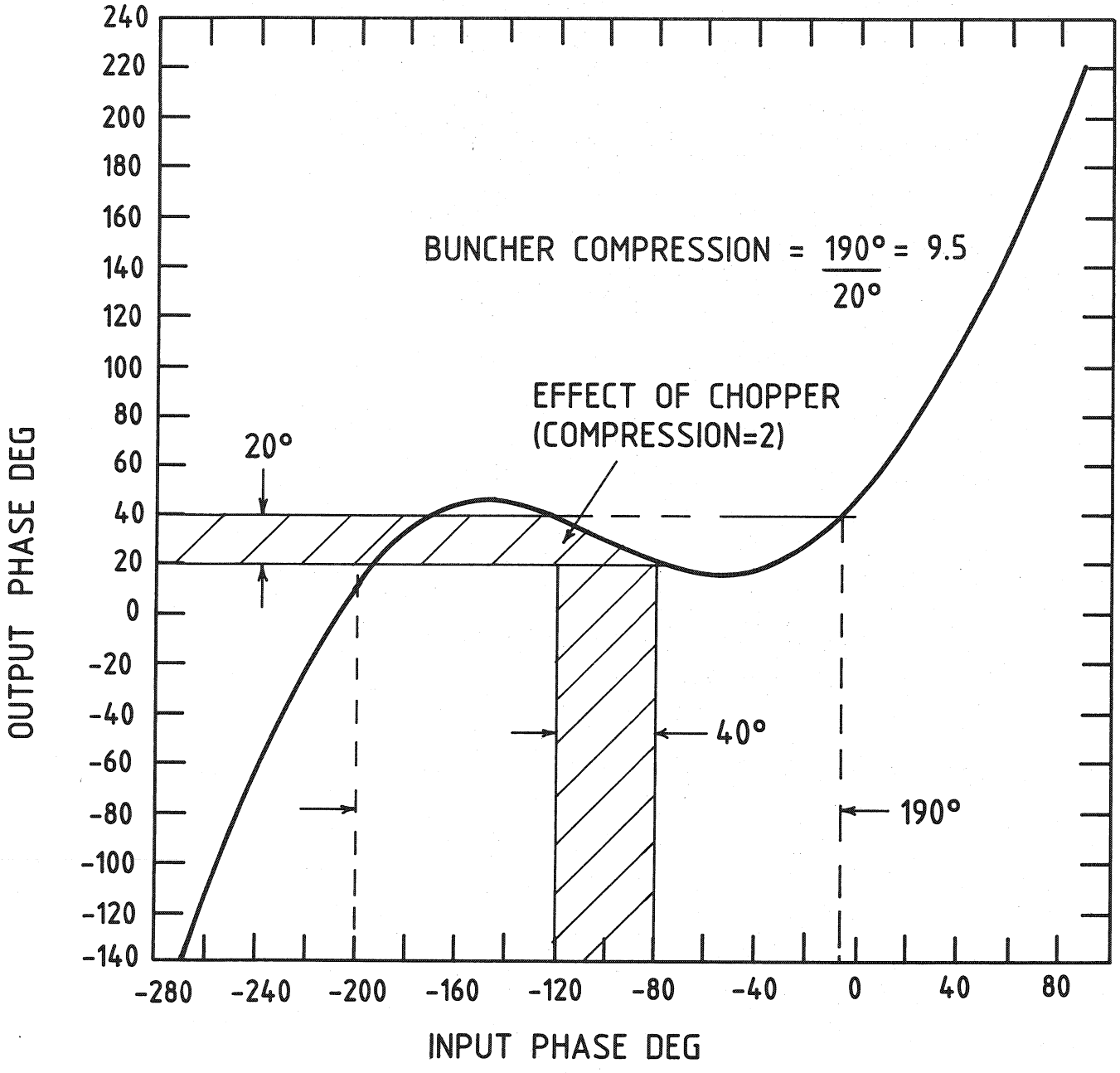

Fig. 14 Calculated beam characteristics at the output of the injector.

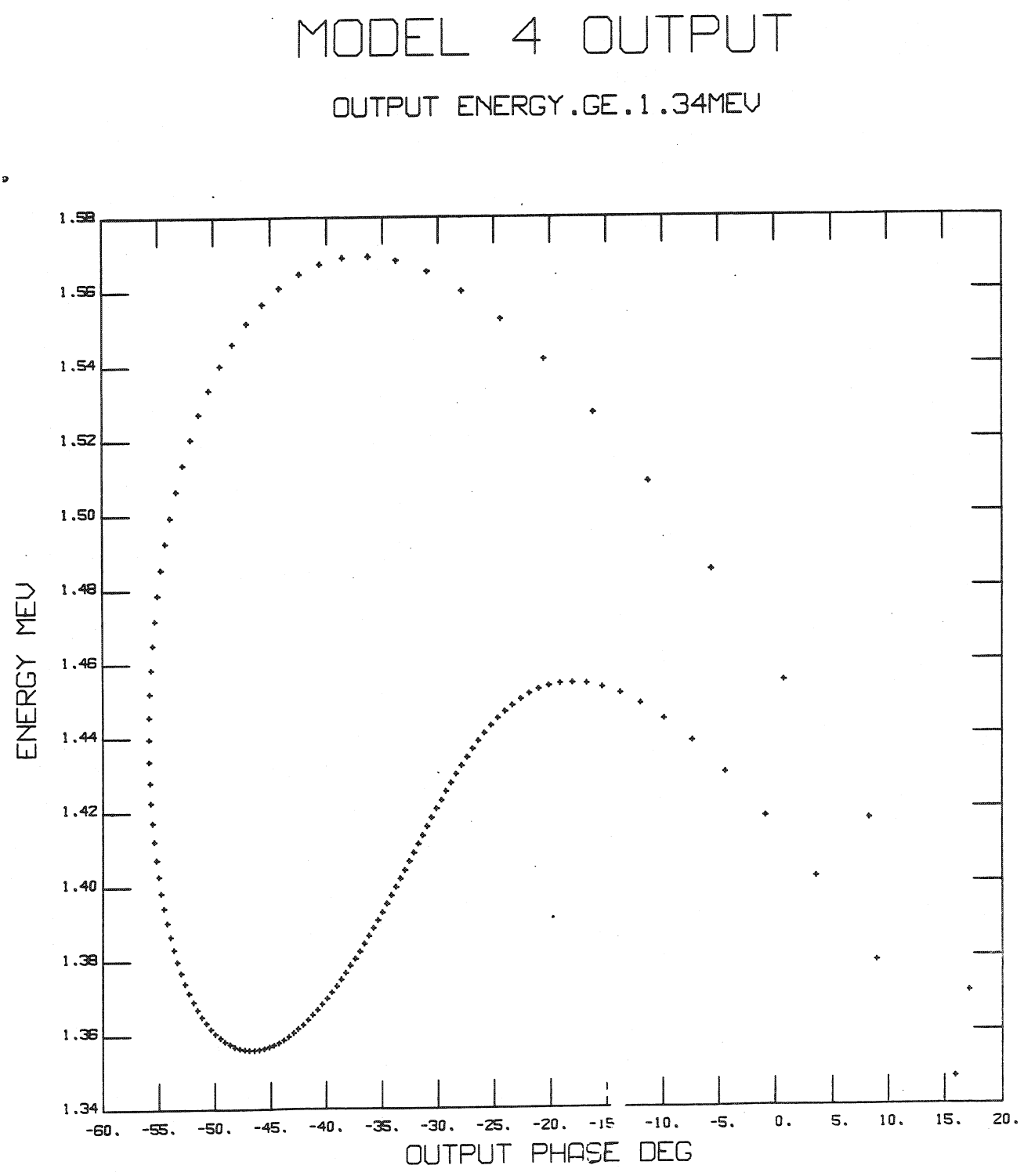

Fig. 15 Calculated beam characteristics at the output of the graded-β linac structure.

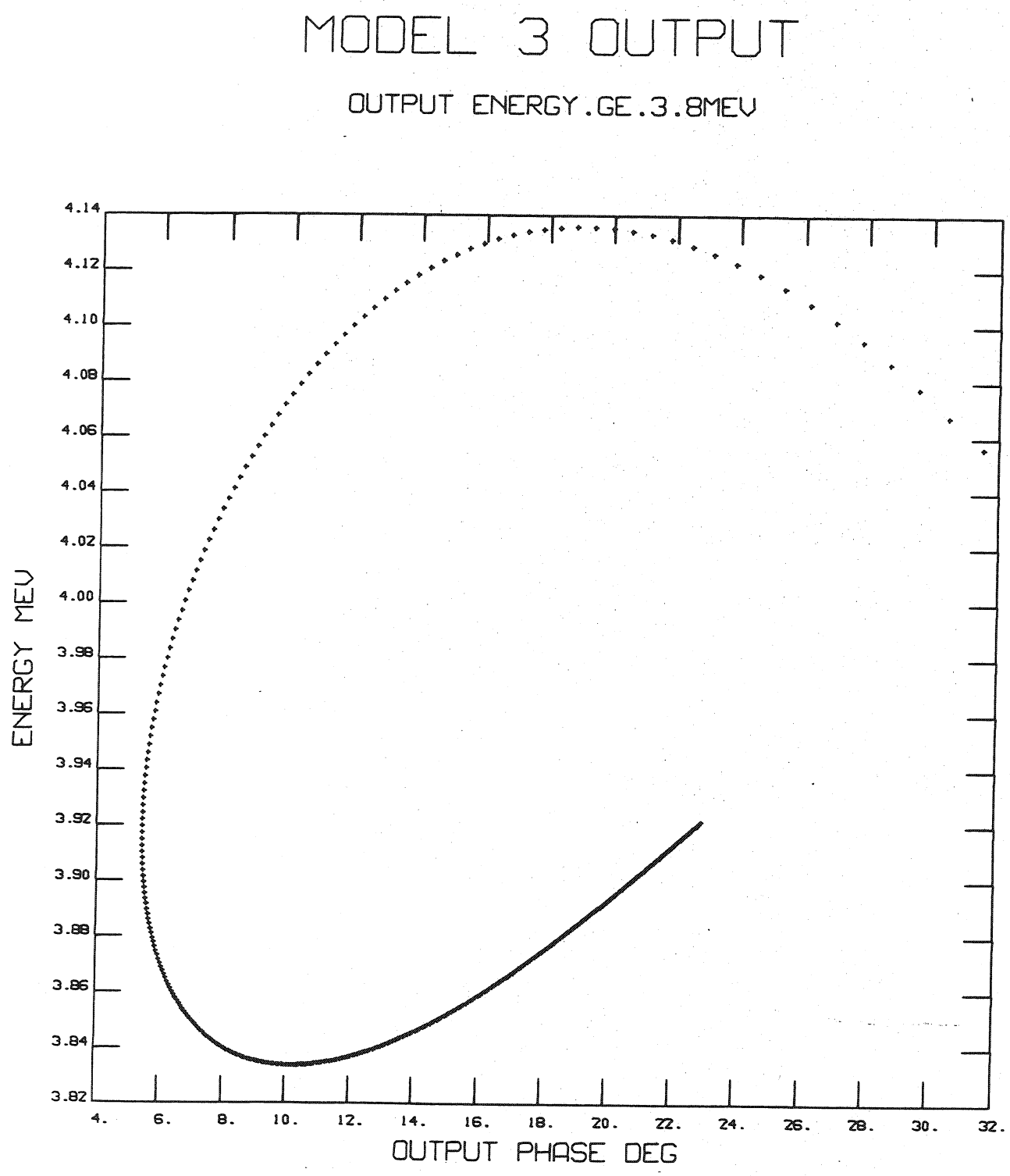

Fig. 16 Calculated beam characteristics at the output of the β=1 linac structure.

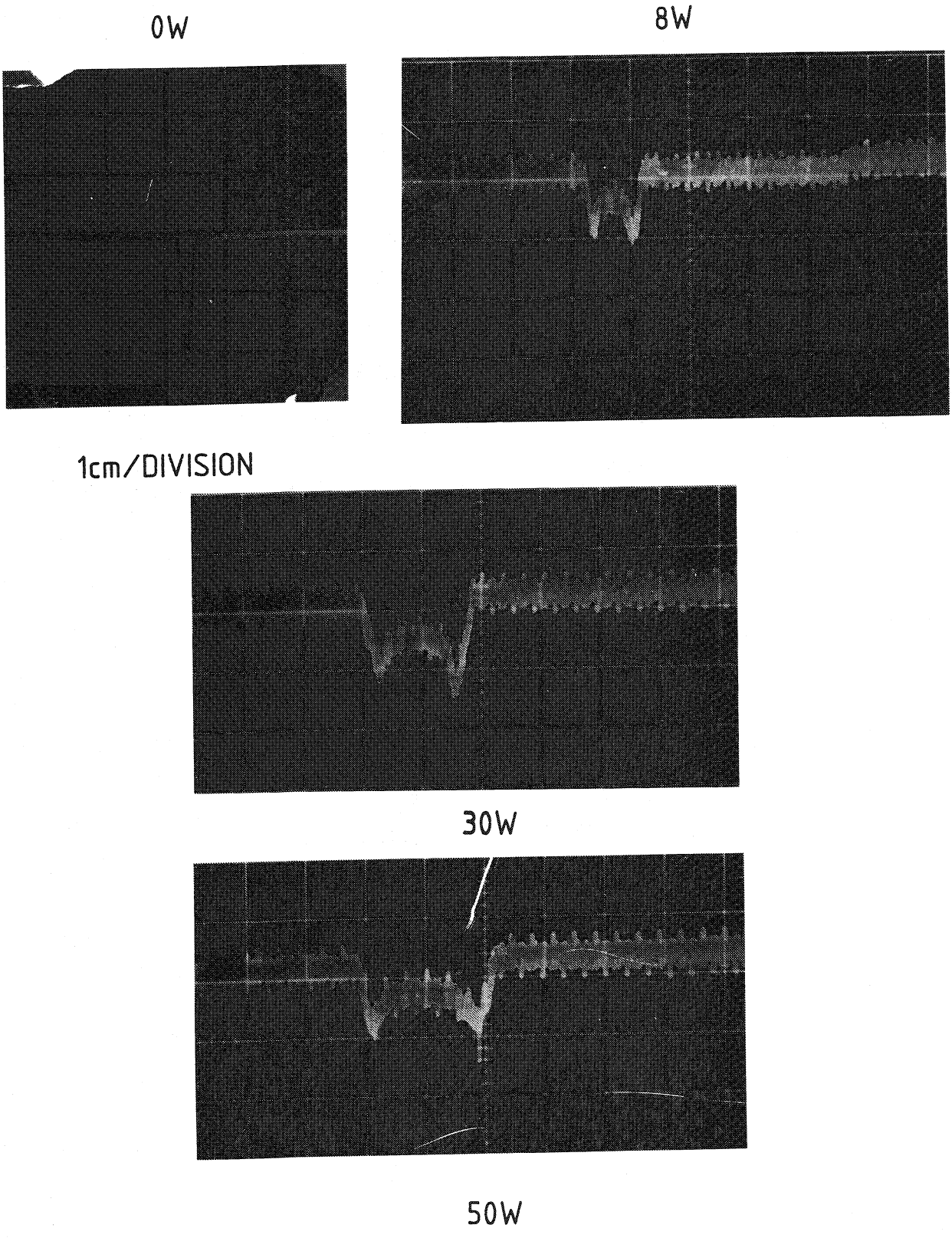

Fig. 17 Transverse dc beam width at various power levels in the chopper cavity.

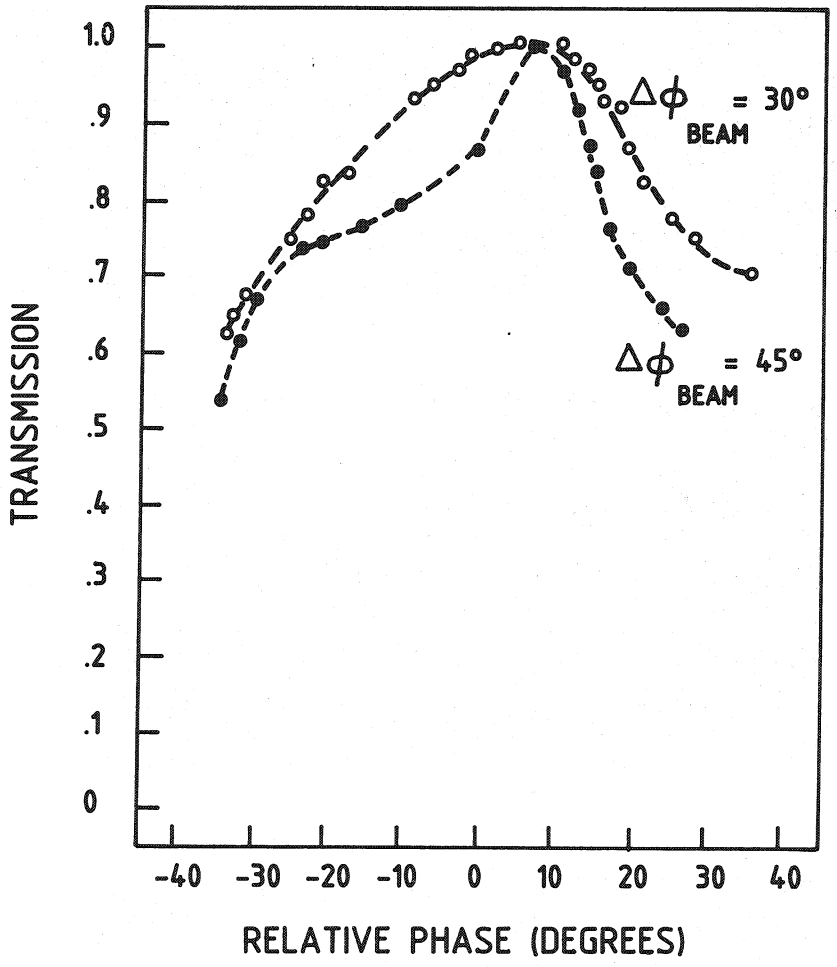

Fig. 18 Transmission through the graded-β linac structure.

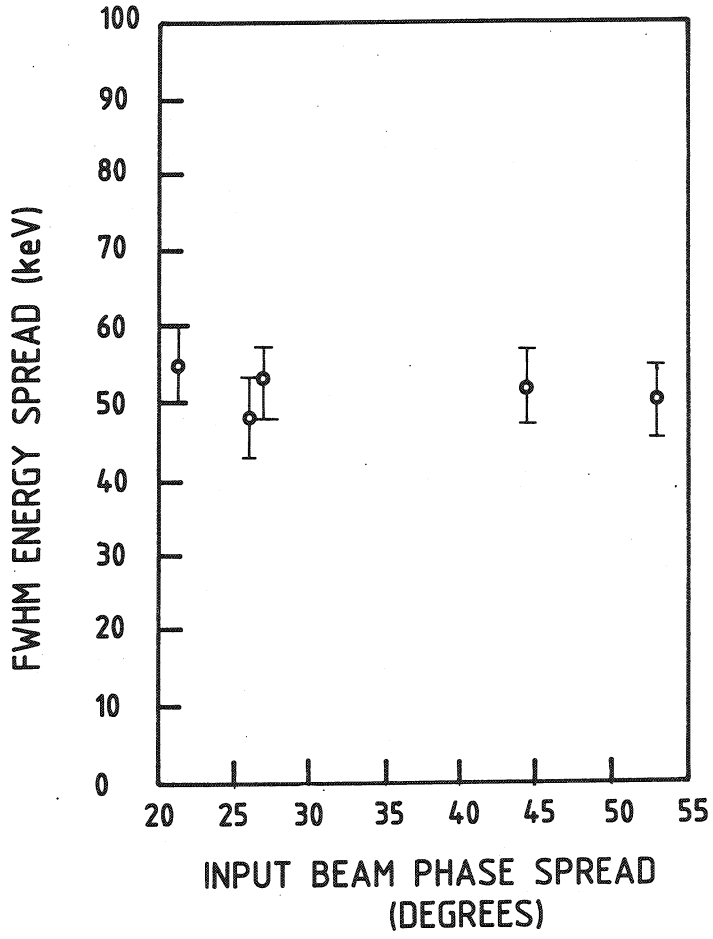

Fig. 19 FWHM output beam energy spread as a function of the phase spread in the injector.

ISSN 0067 - 0367

To identify individual documents in the series we have assigned an AECL- number to each.

Please refer to the AECL- number when requesting additional copies of this document

from

Scientific Document Distribution Office
Atomic Energy of Canada Limited
Chalk River, Ontario, Canada
K0J 1J0

Price: $3.00 per copy

ISSN 0067 - 0367

Pour identifier les rapports individuels faisant partie de cette série nous avons assigné un numéro AECL- à chacun.

Veuillez faire mention du numéro AECL- si vous demandez d'autres exemplaires de ce rapport

au

Service de Distribution des Documents Officiels
L'Energie Atomique du Canada Limitée
Chalk River, Ontario, Canada
K0J 1J0

Prix: $3.00 par exemplaire

1426-86